THE JOURNAL OF PHYSICAL CHEMISTRY B

ARTICLE

pubs.acs.org/JPCB

Effect of Curvature on Nanoparticle Supported Lipid Bilayers Investigated by Raman Spectroscopy

Selver Ahmed,[†] Zhorro Nikolov,[‡] and Stephanie L. Wunder[†]

[†]Department of Chemistry, Temple University, Philadelphia, Pennsylvania 19122, United States

[‡]College of Engineering, Drexel University, Philadelphia, Pennsylvania 19104, United States

ABSTRACT: The packing of lipids on silica (SiO_2) nanoparticles (NPs) was investigated by Raman spectroscopy for 1,2-dipalmitoyl-*sn*-glycero-3-phosphocholine (DPPC) and 1,2-distearoyl-*sn*-glycero-3-phosphocholine (DSPC) as a function of their size, for SiO_2 NPs of 5, 15, 25, 45, and 100 nm nominal diameter. Raman spectral indicators in the C−C and C−H stretching regions were used to determine conformational order and alkyl chain packing for these systems. As the ratio of NP to lipid size decreases, packing in a normal bilayer configuration increases free volume and decreases hydrophobic interaction between the chains. For the 15, 25, 45, and 100 nm SiO_2, for which single supported lipid bilayers (SLBs) are formed around the NPs, the Raman data indicate that there is increased interdigitation and increased lateral packing order between the chains with decreasing NP size, which improves hydrophobic association and decreases the voids that would occur for normal bilayers. For the same size NP, there is increased interdigitation and lateral packing for the DSPC compared with DPPC lipids, as expected based on the greater void volume that would be created for the longer alkyl chain lengths. Another mechanism for filling this void space is the formation of gauche kinks for the terminal methyl groups at the center of the bilayer, which can be monitored by a Raman band at 1122 cm^{-1}. These gauche defects are most prevalent for the largest size (100 nm) NPs but are observed for all NP sizes. For the 5 nm SLBs, which form aggregates, we hypothesize that bilayer bridging can occur between the NPs. Compared with the 15 nm NPs, the order parameter increases but there are fewer trans conformers, possibly due to chains that are loosely packed or isolated in the interstitial regions.

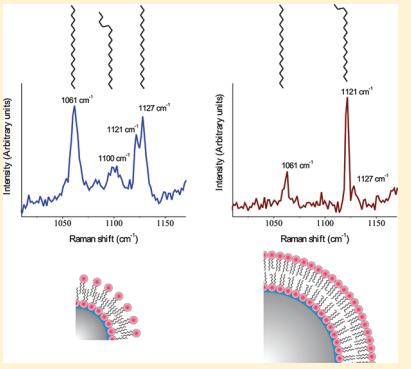

INTRODUCTION

Raman spectroscopy has frequently been used to investigate the conformational order, packing and phase transition temperatures of lipid multilamellar (MLVs) and small unilamellar (SUVs) vesicles, due to the weak Raman scattering of water compared with its strong IR absorption.[1−4] The backbone skeletal (C−C) vibrations have been used as indicators of trans−gauche isomerization,[5] and the CH stretching region at 2800−3100 cm^{-1} has been shown to be sensitive to both intra- and interchain effects.[6] The recent interest in inorganic nanoparticles and their interaction with lipids also makes Raman scattering a technique of choice for monitoring phase transitions, conformational order and packing of lipids on supported lipid bilayers (SLBs), since materials such as silica (SiO_2) also have strong IR absorptions but are weak Raman scatterers. Planar supported lipid bilayers have been investigated by total internal reflection (TIR) Raman spectroscopy,[7] and a micro-Raman/atomic force microscope (AFM) system has been developed that can measure the Raman spectra of multibilayers.[8] However, the high surface area of nanoparticles significantly enhances the ability to measure the Raman spectra of lipids on these surfaces and to investigate the effects of surface curvature.

The packing of lipids as a function of curvature is important for biological events such as budding and fusion of cellular membranes, for which lipid vesicles are often used as surrogates. There thus has been interest in the different packing of lipids on high curvature SUVs compared with low curvature MLVs. Early work comparing Raman spectra of MLVs and SUVs, where the latter have smaller radii of curvature, indicated only slightly lower but broader gel-to-liquid crystal phase transition temperatures (T_m) for the SUVs[9] and greater trans−gauche isomerization for the SUVs in the gel phase, as monitored by the C−C skeletal vibrations.[10,11] Further, in the 2800−3100 cm^{-1} spectral region, which is sensitive to both intra- and interchain effects, MLVs exhibited greater lateral packing order.[10−12] Phase transition temperatures and enthalpies were lower for SUVs compared with their fusion products, large unilamellar vesicles (LUVs), both of which were different than MLVs.[13,14] However, SUVs fuse with time,[13,15] making it more difficult to maintain their size and measure size dependent effects. By contrast, nanoparticles have fixed geometries, so that it is possible to investigate the packing and order of lipids as a function of curvature.

There is some evidence that curvature can induce lipid interdigitation,[16] although interdigitation is typically brought about by addition of small molecules that separate the headgroups.[17] For lipids on solid nanoparticle (NP) supports, as the

Received: June 26, 2011
Revised: August 22, 2011
Published: September 20, 2011

underlying curvature increases and the nanoparticle and lipid dimensions become similar, the minimum energy configuration is not one in which the lipids form a traditional bilayer around the nanoparticles. The latter packing arrangement becomes increasingly unstable due to the large free volume increase if the lipids pack in a "spokes on a wheel" geometry, exposing the hydrophobic alkyl tails to the surrounding aqueous media. One way of mitigating this effect is for lipid interdigitation to occur, as we have proposed using data from nanodifferential scanning calorimetry (nano-DSC).[18] Lipid interdigitation has been investigated by Raman spectroscopy for glycerol induced interdigitation,[19] where increased lateral order was observed for the interdigitated structures, and for binary mixtures of 1-stearoyl-2-caprylphosphatidylcholine(DSPC) /dimyristoylphosphatidylcholine (DMPC), where mixed interdigitated phases (3 acyl chains/headgroup) were proposed.[20] Another mechanism to fill the free volume void is for the ends of the chains near the bilayer center to deviate from a trans configuration of the alkyl chains.

In this work, conformational order and packing are investigated for 1,2-dipalmitoyl-sn-glycero-3-phosphocholine (DPPC) and 1,2-distearoyl-*sn*-glycero-3-phosphocholine (DSPC) supported lipid bilayers (SLBs) on monolithic silica (SiO_2) nanoparticles with nominal diameters of 5, 15, 25, 45, and 100 nm. In particular, the conformationally dependent bands in the optical skeletal region and the bands in the methylene bending and stretching regions that are sensitive to lateral packing order are investigated. We have paid particular attention to a vibration at 1122 cm^{-1}, attributed to alkyl chains with a single gauche rotation of the terminal methyl group near the bilayer center,[21] and to a comparison of lateral packing for alkyl chains both as a function of nanoparticle size and for different length alkyl chains on the same size SiO_2.

EXPERIMENTAL SECTION

Materials. 1,2-Dipalmitoyl-*sn*-glycero-3-phosphocholine (DPPC; 16:0 PC) and 1,2-distearoyl-*sn*-glycero-3-phosphocholine (DSPC; 18:0 PC) were obtained from Avanti Polar Lipids (Alabaster, AL) and used without further purification. Snowtex colloidal silica (SiO_2) beads with nominal diameters of (i) 4−6 nm (referred to as 5 nm), ST-XS, 20.3 wt % SiO_2, lot 150509, pH 9.2, specific gravity 1.135; (ii) 10−20 nm (referred to as 15 nm), ST-40, 40.8 wt % SiO_2, lot 170916, pH 10.1, specific gravity 1.308; (iii) 20−30 nm (referred to as 25 nm), ST-50, 47.9 wt % SiO_2, lot 170418, pH 8.9, specific gravity 1.372; (iv) 40−50 nm (referred to as 45 nm), ST-20 L, 20 wt % SiO_2, lot 170211, pH 9.5−11.0, specific gravity 1.12−1.14; and (v) 100 nm, MP-1040, 40.7 wt % SiO_2, lot 170425, pH 9.3, specific gravity 1.300, were kindly donated by Nissan Chemical Industries, Ltd. (Japan) and used as-received. The SiO_2 beads were prepared by the water glass process and had densities of 2.2−2.6 g/cm^3 (reported by manufacturer). The beads are prepared at a specific size, in the size range given by the manufacturer. DLS and TEM data for these beads have been reported previously.[18] All solutions/suspensions were prepared with HPLC grade water and chloroform, purchased from Fisher Chemicals (Fairlawn, NJ). A 0.1M, pH 8.0 buffer was made from $Na_2HPO_4 \cdot 7H_2O$ and $NaH_2PO_4 \cdot H_2O$ (PBS) and 75 mM NaCl. An Avanti Mini-Extruder from Avanti Polar Lipids was used for extrusion of the lipids.

Preparation of Supported Lipid Bilayers (SLBs). Appropriate amounts of lipid were dissolved in chloroform. Dry lipid films were formed after evaporation of the solutions under a stream of nitrogen and then in a vacuum oven overnight to remove any residual solvent. The lipid film was redispersed in buffer and incubated at a temperature (60 °C for DPPC, 70 °C for DSPC) above the T_m of the lipids for a minimum of 2 h with periodic shaking to form hydrated multilamellar vesicles. SUVs were obtained from MLVs by subjecting them to 5 freeze/thaw cycles followed by extrusion using a polycarbonate filter with pore sizes of 50 or 100 nm. SUV sizes of ∼60 and 100 nm were measured by dynamic light scattering (DLS).[18] Approximately 1 mL of a 5−10 mg/mL lipid solution was passed back and forth for up to 50 times. Although a clear solution was obtained after 20 passes, the vesicles became more monodisperse as the number of passes increased.[18] Assuming no loss of lipid during the extrusion process, additional buffer was added to the extrusion product to yield vesicle solutions of ∼2 mg/mL lipid.

Adsorption of the vesicles onto the beads to form supported lipid bilayers was accomplished by addition of the SiO_2 dispersions to the vesicle solutions held above T_m, so that there was approximately at least a 2-fold, and up to a 5-fold excess of lipid necessary to form a bilayer on the beads. Typical preparations involved addition of 40−90 μL bead dispersions to 5−25 mL lipid solution. The pH of the mixture remained buffered at pH 8.0. These mixtures were incubated for 2 h at 50 °C for DPPC, and 65 °C for DSPC, and then allowed to cool to room temperature (RT). The lipid coated beads were centrifuged at 3900 rpm using a Fisher Scientific Marathon 3200 centrifuge, and the supernate decanted. Additional water was added to the pellet, and the centrifuge/washing steps repeated 3 times. After the last centrifugation the pellet was redispersed in 300 μL D_2O.

Raman and Nano-Differential Scanning Calorimetry Data. Raman spectroscopy analysis was performed using a micro-Raman spectrometer (Renishaw, RM 1000) with a 514.5 nm air-cooled Ar ion laser source and a 1800 lines/mm grating polychromator with RenCam CCD detection, providing a resolution of 1 cm^{-1}. The laser source was focused on the sample nanoparticle suspension through a long working distance 50× objective to a spot size of approximately 2 μm diameter and the Raman signal from the MLVs, SUVs and SLBs was collected in a back scattering geometry. A Linkam THMS600 heating stage was used for temperature control with 0.1 °C accuracy of the nanoparticle suspensions during phase transition studies. In those cases Raman spectra were recorded after allowing for 10 min thermal equilibrium to be achieved at every temperature point.

The acquisition time for Raman spectra was between 10 and 20 min depending on the strength of the Raman signals until a satisfactory signal-to-noise ratio was achieved. It was found that SLBs in smaller particle size suspensions, due to their higher surface areas per unit volume, produce much stronger Raman signals. Therefore longer accumulation times were needed in the case of suspensions of bigger diameter nanoparticles and also when collecting spectra in the fingerprint region 650−1800 cm^{-1}, where the band intensities were much weaker than in the stretching region (2700−3200 cm^{-1}). Possible laser heating effects during the Raman spectral collection were eliminated by limiting the argon laser power density to levels where it was proven that the spectra are not affected by prolonged irradiation. Data analysis was performed using the Renishaw Wire 2.0 software.

Nanodifferential scanning calorimetry (nano-DSC) measurements were obtained on a TA Instruments (New Castle, DE) Nano DSC-6300. Samples were placed in the nano-DSC at RT,

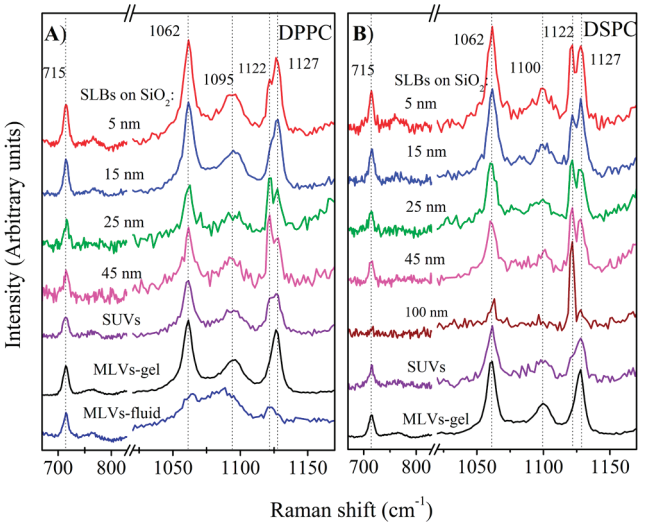

Figure 1. Raman spectra at RT in the headgroup and skeletal optical (C−C stretch) region of (A) DPPC MLVs, SUVs, and SLBs on 5, 15, 25, and 45 nm SiO_2, and in the melt of MLVs; and (B) DSPC MLVs, SUVs, and SLBs on 5, 15, 25, 45, and 100 nm SiO_2. Dotted lines indicate spectral bands discussed in paper.

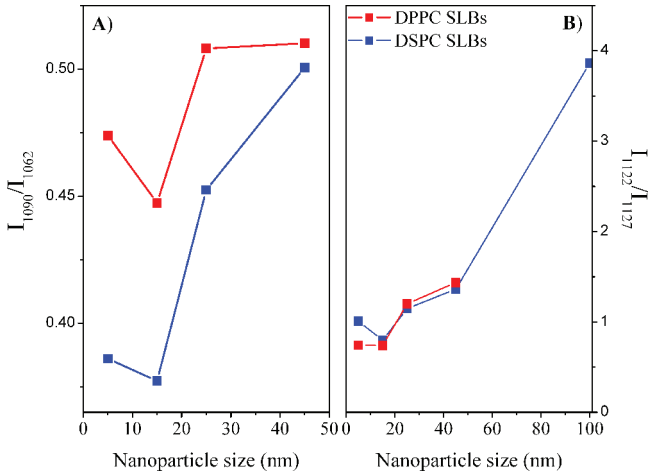

Figure 2. (A) Plot of I_{1090}/I_{1060} for DPPC and DSPC SLBs at RT as a function of SiO_2 size; (B) plot of I_{1121}/I_{1127} for DPPC and DSPC SLBs at RT as a function of SiO_2 size.

cooled to 5 °C and heated/cooled from 5 to 35 at 1 °C/min. The second heating scans are reported. TEM measurements were made on a FEI Technai 12T electron microscope with an operating voltage of 120 KeV. Images were captured using a Gatan DualVision 300 (1k), side-entry cooled CCD camera. Image capture, processing and analysis were performed with Gatan "Digital Micrograph" software.

RESULTS AND DISCUSSION

Headgroup and C−C Vibrations. The most intense headgroup vibration in phosphatidyl cholines (PC) is a C−N stretching mode, which appears between ~714−722 cm^{-1}, and which we observe for DPPC, DSPC MLVs, SUVs, and their SLBs at 718−722 cm^{-1} (Figure 1, panels A and B). The frequency of this band is insensitive to any conformational change of the alky chains associated with melting for the MLVs, SUVs and SLBs. However, choline vibrations are sensitive to the conformation of the O−C−C−N^+ backbone. The totally symmetric stretch of C−N for the quaternary ammonium group appears at 720 cm^{-1} for the gauche and at 770 cm^{-1} for the trans conformation.[22] Here, the intensity of the 720 cm^{-1} vibration is greater than that of a very weak 770 cm^{-1} vibration in all the Raman spectra, indicating that the orientation is predominantly gauche around the O−C−C−N^+ group, consistent with previous observations.[22]

The hydrocarbon skeletal C−C stretching region, which extends from 1000−1150 cm^{-1}, provides the most convenient spectral region for observing changes of the acyl chains in phosphatidylcholine bilayers,[3−5] although there is also a minor contribution from the PO_2^- symmetric stretch in the 1100 cm^{-1} region[3]. The ν(C−C) modes are sensitive to true gauche and trans conformations of the methylene chain, and are much less affected by methylene rotations or other bond deformations.[23] In the current work (Figure 1, panels A and B), vibrations at 1061, 1100 (DSPC) or 1096 (DPPC), consistent with the chain length dependence of the middle peak,[24] and 1121/1127 cm^{-1} are observed in the gel phase of DPPC and DSPC, and at 1065, 1087, and 1122 cm^{-1} in the liquid crystalline phase.

Band assignments have been made for IR and Raman vibrations of short and long $CH_3-(CH_2-CH_2)_n-CH_3$ chains, where n is the number of ethylene units, using normal coordinate analysis,[25−27] and by analogy, with lipid bilayers.[3] In the case of all trans chains, the chain length independent vibrations occur at ~1064 (out-of-phase, asymmetric C−C stretch) and 1130 cm^{-1} (in-phase, symmetric C−C stretch).[27] The 1130 cm^{-1} band arises from all-trans segments,[27] whereas the 1064 cm^{-1} band is sensitive to the presence of gauche defects.[28] There is also a weak mode between 1075 and 1100 cm^{-1} that increases with *n*. In the gel phase of hydrated, saturated lipids, three peaks are usually observed, at 1060, 1000, and 1127 cm^{-1}, with the assignments of the 1060/1127 cm^{-1} bands the same as for alkanes, and the 1100 cm^{-1} band attributed to all trans chains with a single gauche defect.[24] The presence of this peak in the gel phase indicates that DPPC (or DSPC) is never "all-trans" but possesses some gauche conformers that have been suggested to be located at the end of the acyl chains, and thus at the bilayer center.[24] IR CD_2 substitution data combined with models of disorder in the hexagonal (rotator) phase of alkanes indicate that disorder is the result of g-t-g′ kinks, in which the probability of occurrence is greatest at the ends.[29]

Upon melting of alkane/polyethylene chains, or at the gel-to-liquid crystal transition in lipids, the intensity of the 1064 and 1130 cm^{-1} bands decrease, and the 1100 cm^{-1} band shifts and merges with a new broad intense band at 1090 cm^{-1}, as shown here for DPPC in the high temperature fluid phase. These changes occur due to a decrease in the number of all trans segments and to the appearance of chain segments containing gauche rotations along the chain.[30] Ab initio calculations indicate that eight to ten contiguous CH_2 units are required in order that a sequence contribute most of its intensity to the 1064/1130 cm^{-1} vibrations; shorter sequences make intensity contributions to these vibrations as well as to the 1090 cm^{-1} mode.[31] Further, it has been shown that intensity reduction is greater for the 1130 cm^{-1} than for the 1060 cm^{-1} vibration with introduction of gauche defects;[32] for example, the intensity of the 1130 cm^{-1} wavenumber band was reduced for alkyl chains on transition from the orthorhombic to the hexagonal phase, but the decrease

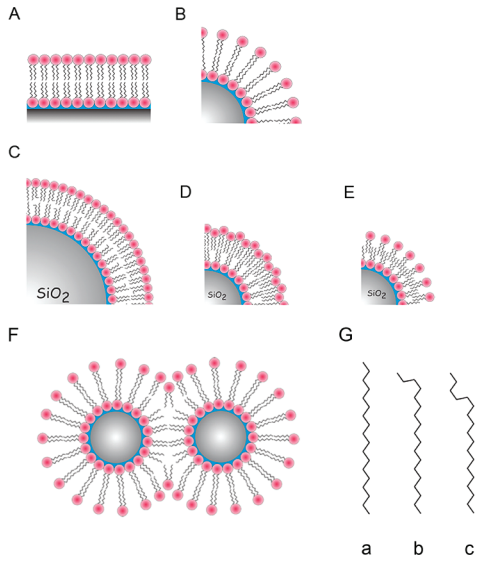

Figure 3. Schematics of lipids forming (A) bilayers on a planar substrate; (B) bilayers on highly curved SiO_2 nanoparticles, where the dimensions of the lipids become similar to the underlying support; (C) bilayers in which the alkyl chains contain a gauche kink at the terminal methyl group; (D and E) increasingly interdigitated structures; (F); bridged structures, in which each half of bilayer is on an adjacent SiO_2 NP; (G) alkyl chain conformations- (a) all trans chain, (b) chain with terminal methyl group and (c) chain with gauche defects separated by trans conformation.

was not linearly proportional to the number of gauche bonds introduced, but instead resulted from a low concentration of gauche bonds.[33] MD simulations and IR data that are based on spatially localized C−C vibrations indicate that Raman spectra in this region overestimate the number of gauche bonds.[34] Further, these calculations indicate that for constrained alkyl chains in lipids compared with unconstrained alkanes, the short conformational sequences are similar, but there are more long all-trans sequences for the lipids.[34]

The amount of alkyl chain disorder is often taken as the relative number of gauche/trans conformers, measured by their Raman intensity ratios $I[\nu(C-C)_G]/I[\nu(C-C)_T] = I_{1090}/I_{1060}$. This is shown in Figures 2A for DPPC and DSPC SLBs at room temperature as a function of SiO_2 size. Unlike alkanes such as octadecane, where the number of gauche bonds is zero in the crystalline phase,[23] all of the SLBs have gauche conformations in the RT gel phase. The number of gauche rotamers increases as the nanoparticle size increases, with the exception of the smallest nanoparticle size, and is greater for DPPC than for DSPC for the same size nanoparticle. Thus there are more trans segments on the smaller NP SiO_2 and for longer alkyl chains. One way to understand these trends is based on the necessity of increasing hydrophobic interactions between the alkyl chains. As shown schematically in Figure 3, if both the lipid headgroups and alkyl chains pack as on a planar surface, the resultant "spokes on a wheel" geometry would decrease the hydrophobic interactions between the alkyl chains. Since free volume increases as the lipid dimensions approach the NP dimensions, the chains must adopt configurations that mitigate this effect. One way to fill the "voids" is the formation of interdigitated structures,[18] which have a greater proportion of trans segments. Although it is possible to observe the lipid bilayer by TEM for DMPC,[35] it is difficult to measure the small differences in bilayer thickness expected for normal and partially interdigitated structures. However, the Raman data suggest that the alkyl tails increasingly interdigitate with decreasing NP size, resulting in more trans segments. Since for the same size SiO_2 NP, there is increasing void space for the longer alkyl chains, increased interdigitation, with the concomitant increased proportion of trans bonds, is expected and observed.

A band at 1121 cm^{-1} is also recorded in the spectra of SUVs and SLBs, either as a distinct band or as a shoulder on the 1127 cm^{-1} vibration. A vibration at ∼1122 cm^{-1} has previously been observed in DMPC, DPPC and DSPC lipid bilayers at temperatures just below T_m and has been assigned to the formation of a single gauche bond rotation of the terminal methyl group oriented toward the center of the bilayer.[6,21,36] What is interesting here is that we observed distinct differences in the intensity ratio of these two bands, I_{1121}/I_{1127}, between the MLVs and SUVs of the same lipid and for the lipid on different size nanoparticles (Figure 1, panels A and B). Only the 1127 cm^{-1} vibration is observed in hydrated MLV spectra at RT for both DPPC and DSPC, indicating a predominance of all trans-chains, while both bands are observed for the DPPC and DSPC SUVs, indicating a greater proportion of chains with a gauche bond rotation of the terminal methyl group. MLVs that have also been freeze thawed, and thus reduced in size, have I_{1121}/I_{1127} ratios intermediate between as prepared MLVs and SUVs (not shown).

In view of its assignment to a terminal gauche defect, it is reasonable that I_{1121}/I_{1127} is less (more all trans chains) for the MLVs than the SUVs. The large (∼1000 nm) MLVs, with almost planar geometries compared with the area of single lipids, have less need to form a terminal gauche defect in the chain to achieve packing of the hydrophobic tails, compared with the ∼50−100 nm SUVs. The formation of this terminal defect may thus be a mechanism by which hydrophobic interchain interactions are increased in the high curvature SUVS. Although previous Raman[12] and deuterium NMR[37] studies showed no differences in trans−gauche isomerism between SUVs and MLVs, other Raman studies suggested that sonication (producing SUVs) decreased interchain interactions, possibly due to imperfect packing toward the center of the bilayer,[12] and the gel-to-liquid crystalline phase transition was broader for SUVs compared with MLVs.[9]

For the SLBs, I_{1121}/I_{1127} decreases for DPPC and DSPC with a decrease in nanoparticle size (Figure 2B; except for the smallest size nanoparticles), which also reflect packing differences for lipids as a function of SiO_2 curvature. The decrease in intensity ratio, I_{1121}/I_{1127}, with decreasing bead size indicates that there are fewer terminal gauche defects and more all-trans segments on the smaller size SiO_2 nanoparticles. This initially seems counterintuitive, since it might be expected, as mentioned in the comparison between MLVs and SUVs where the opposite was observed, that it would be harder to organize the lipids (in straight chain segments) on the smaller size nanoparticles, resulting in more terminal gauche segments. However, unlike MLVs and SUVs, the SLBs are affected by the constraints of the underlying support, in particular, that the headgroups pack as on a planar surface. Therefore, as discussed above for the $I[\nu(C-C)_G]/I[\nu(C-C)_T]$ ratio, and previously reported using nanoDSC data,[18] there is increasing interdigitation (and thus more trans segments) for lipids on SiO_2 nanoparticles with decreasing nanoparticle size. This suggests that there are two ways the alkyl

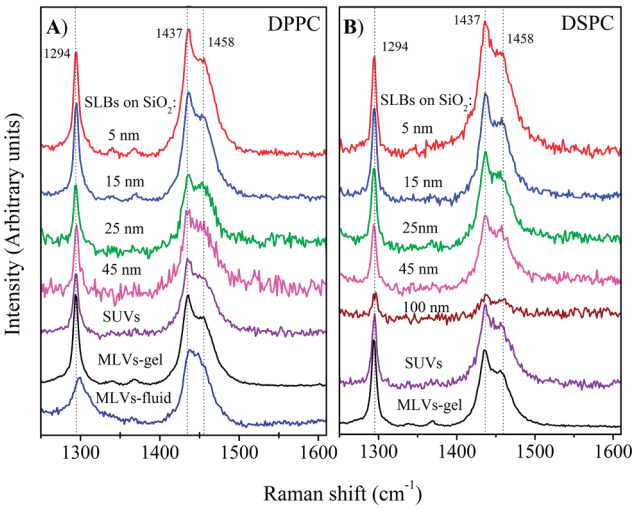

Figure 4. Raman spectra in the CH_2 twisting, wagging and bending region at RT for (A) DPPC MLVs, SUVs, and SLBs on 5, 15, 25, and 45 nm SiO_2 and in the melt of MLVs; (B) DSPC MLVs, SUVs, and SLBs on 5, 15, 25, 45, and 100 nm SiO_2. Dotted lines indicate spectral bands discussed in paper.

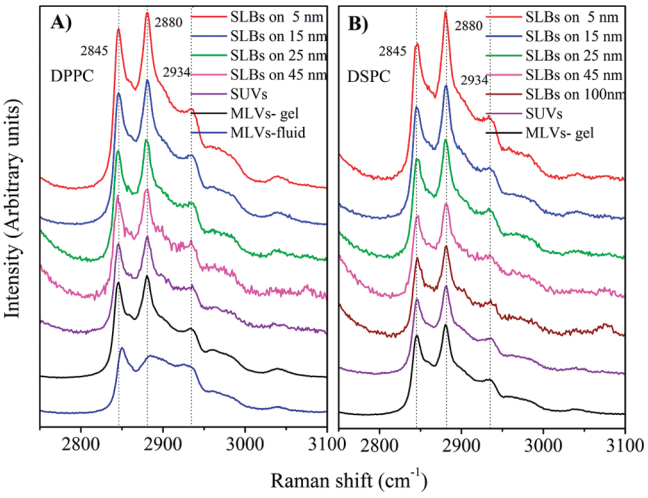

Figure 5. Raman spectra in the CH_2 and CH_3 region at RT for (A) DPPC MLVs, SUVs, and SLBs on 5, 15, 25, and 45 nm SiO_2 and in the melt of MLVs; (B) DSPC MLVs, SUVs, and SLBs on 5, 15, 25, 45, and 100 nm SiO_2. Dotted lines indicate spectral bands discussed in paper.

chains can increase their hydrophobic interactions when packed on solid supports, namely interdigitation, and also the formation of gauche conformers at the ends of the chain that serve to fill in the void space. The latter is more prevalent for the large size SiO_2 NPs, as is apparent for DSPC on the 100 nm SiO_2, where the 1121 cm^{-1} vibration is the most intense band in this spectral region.

CH_2 Twisting/Wagging/Bending (1200−1600 cm^{-1}) Region. The bands in this spectral region (Figure 4) arise from twisting, wagging, and bending modes of the CH_2 group. The band at 1295 cm^{-1} is the CH_2 twist[6] and the weak band at 1370 cm^{-1} is a CH_2 wagging motion.[38] The CH_2 bending region is an indicator of the lattice structure of lipids. It is affected by intramolecular as well as intermolecular Fermi resonance (FR) interactions. Isotopic dilution studies of single all trans alkane chains in a deuterated matrix[39] and model calculations[40] indicate that Fermi resonance interactions between rocking fundamentals (723−735 cm^{-1}) and the unperturbed bending fundamental (1442 cm^{-1}) result in a strong Raman band at 1431 cm^{-1} and a weaker, broader one at 1458 cm^{-1} for the all trans chain. These two vibrations are the only ones observed in an hexagonal lattice,[41] whereas in a monoclinic or orthorhombic lattice, there are further crystal field splitting interactions resulting in an additional band at 1418 cm^{-1}.[39,41] Thus, the spectra of the MLVs, SUVs and SLBs for DPPC and DSPC all indicate that the alkyl chains are in a hexagonal lattice. In the melt, a single broad asymmetric Raman peak at 1440 cm^{-1} is observed, since there are neither inter- nor intramolecular Fermi resonance interactions when gauche bonds are introduced; the asymmetry may arise due to residual trans sequences for the lipids in a confined geometry.

CH_2 and CH_3 Stretching Region 2750−3100 cm^{-1} Region. Both the CH_2 and CH_3 vibrations are in the 2750−3100 cm^{-1} spectral region (Figure 5, panels A and B). The weak band at 2871, $\nu_s(CH_3)^{FR}$, and the one at 2935 cm^{-1}, $\nu_s(CH_3)^{FR}$, are the methyl symmetric stretches (r^+) in Fermi resonance with an overtone transition of the CH_3 asymmetric deformation mode.[42] The antisymmetric methyl stretches, $\nu_a(CH_3)$, appear at 2952 (r_b^-, out-of-skeletal plane asymmetric stretch) and 2964 cm^{-1} (r_a^-, in-skeletal plane asymmetric stretch),[39] whereas the antisymmetric methyl stretch of the choline headgroup appears at 3042 cm^{-1}.[3,43]

The methylene vibrations are sensitive to conformational changes as well as intermolecular interactions of alkanes, polyethylene and the alky chains of lipids. The CH_2 antisymmetric stretch (d^-) is coupled to rigid rotations/torsional vibrations,[44,45] so that it broadens considerably as the temperature increases, as observed in the hexagonal, and then melt phase,[44] and increases continuously in frequency, from 2884 cm^{-1} (crystal) to 2898 cm^{-1} (melt) as gauche conformers are introduced.[44]

The symmetric CH_2 stretch (d^+) is complex due to extensive Fermi resonance interactions between the symmetric stretching fundamental and a continuum of overtones of the bending modes both for the extended[46] and disordered chain,[47] as well as from interchain interactions. For single (isotopically isolated), all trans chains, the Fermi resonance interactions result in a strong 2845 cm^{-1} band (d_{FR}^+), and two broader bands, at 2890 cm^{-1} (d_{FR}^+) (underlying the asymmetric stretch) and a less intense band at ~2930 cm^{-1} (d_{FR}^+); most of the intensity of the symmetric stretch is in the broad bands.[39] In the isotropic spectra of highly oriented polyethylene (few CH_3 groups) or CD_3 terminated alkanes, the bands occur near 2850, 2900, and 2925 cm^{-1}, and at similar frequencies in the melt, but with different intensity ratios.[47] Thus the broad band often referred to as 2935 cm^{-1} has contributions from Fermi resonances of the symmetric methylene stretch at 2922 cm^{-1} (d_{FR}^+), which is affected by methylene chain conformation,[40] and the methyl stretch (r_{FR}^+) of the alkyl chains at 2938 cm^{-1}, which is not[42,47] In particular, the 2922 cm^{-1} (d_{FR}^+) component of the symmetric CH_2 stretch increases with respect to the 2950 cm^{-1} (d_{FR}^+) component as gauche conformers are introduced in the chains,[47] as shown here for DPPC MLVs (Figure 5A) or SLBs (Figure 6).

In the hexagonal rotator phase of alkanes, the Raman spectrum is intermediate between that of the orthorhombic crystal and an isotopically diluted all trans chain, suggesting some (but less than for orthorhombic) perpendicular dispersion,[39] and is most similar to that of lipid vesicles. As in the case of the CH_2 bending

region, the CH stretching region indicates that the alkyl chains are in a hexagonal packing arrangement in the MLVs, SUVs and SLBs for DPPC and DSPC.

Phase Transitions of SLBs. Temperature dependent Raman spectra in the CH stretching region are shown in Figure 6 for DPPC on 15 nm SiO_2. As has been observed for MLVs, with increased temperature the antisymmetric CH_2 stretch, ν_a (CH_2), at 2884 cm^{-1} increases in frequency to 2890 cm^{-1}, and is reduced in height compared with one component of the symmetric CH_2 stretch, ν_s^{FR} (CH_2), at 2845 cm^{-1}. This ν_s^{FR} (CH_2) vibration increases in frequency from 2847 to 2852 cm^{-1} with increasing temperature. The ν_s^{FR} (CH_2, CH_3) symmetric stretch at 2922−2935 cm^{-1} (also contains CH_3 component, see above) increases in intensity with respect to both the ν_s^{FR} (CH_2) = 2845 and ν_a (CH_2) = 2884 cm^{-1} bands. The decreased height of the ν_a (CH_2) = 2884 cm^{-1} vibration arises both from temperature induced broadening and also because of Fermi resonance changes in the symmetric stretches, which result in reduction in intensity of the ν_s^{FR} (CH_2) = 2900 cm^{-1} band (thus lowering the 2884 cm^{-1} band that sits on top of the ν_s^{FR} (CH_2) = 2900 cm^{-1} mode) and an increase in the intensity of the ν_s^{FR} (CH_2, CH_3) = 2922−2935 cm^{-1} band. The ν_s^{FR} (CH_2) = 2922 cm^{-1} band increases with respect to the ν_s^{FR} (CH_2) = 2845 cm^{-1} as gauche conformers are introduced into the chain, due to Fermi resonance effects[45] and to the upward shift in frequency and broadening of the ν_a (CH_2) = 2884 cm^{-1} band. At high (~60 °C) temperatures after melting (T_m = 39−41 °C), it is difficult to distinguish the ν_a (CH_2) = 2890 cm^{-1} and the ν_s^{FR} (CH_2) = 2900 cm^{-1} vibrations.

Spectroscopic determination of phase transition temperatures is often derived from intensity ratios of bands in the CH stretching region, since these are the most intense vibrations in the Raman spectra of alkyl chains.[6,48] The intensity ratios often used are $I_{2845}/I_{2884} = I[\nu_s^{FR}(CH_2)]/[I(\nu_a(CH_2)]$, $I_{2935}/I_{2884} = I[\nu_s^{FR}(CH_2,CH_3)/I(\nu_a\ (CH_2)]$, and $I_{2935}/I_{2845} = I[\nu_s^{FR}(CH_2, CH_3)/I(\nu_s^{FR}\ (CH_2)]$. Alternatively, a lateral order parameter[11]

$$S_{lateral} = (r(\text{sample}) - 0.7)/1.5 \text{ and } r = I_{2884}/I_{2845}$$

is defined, so that S = 1 for a chain in a crystal (r = 2.2) and S = 0 for a chain in the liquid state (r = 0.7),[11] although there are difficulties with use of this relationship,[39,48] and all of the indicators are only qualitative measures of lateral order or packing.

Plots of the above spectral indicators for DPPC on 4−5, 10−20, 20−30, and 40−50 nm SiO_2 as a function of temperature are shown in Figure 7. In comparison with data for MLVs, which all exhibit a more pronounced sigmoidal character over a narrower temperature range,[49] all of the plots show changes over a broader temperature range, at phase transition temperatures around 39−40 °C, in the temperature range expected based on previous nanodifferential scanning calorimetry data.[18] These results are in agreement with phase transitions measured by Raman spectroscopy for DMPC planar supported lipid bilayers,[7] which exhibited broader transition widths than MLVs, and with earlier Raman data for DMPC and DPPC SUVs, in which the transitions were broader for SUVs than for MLVs and without pretransitions.[11]

Lateral Order. The degree of lateral order, $S_{lateral}$ is compared as a function of nanoparticle size at RT for both DPPC and DSPC SLBs, and is observed to increase with decreasing SiO_2 size (Figure 8A). For the same size SiO_2 nanoparticle, lateral order is greater for the longer alkyl chain DSPC than for the shorter alkyl chain DPPC. In order to correlate conformational disorder to lateral packing, I_{1060}/I_{1090} (or the inverse) versus $S_{lateral}$ can be plotted.[23,50] When conformational disorder is measured by gauche bond content, $I[\nu(C-C)_G]/I[\nu[(C-C)_T]$, and plotted as a function of $S_{lateral}$ for different size SiO_2 nanoparticle SLBs at RT (Figure 8B), the lateral order decreases/increases as more gauche/trans bonds are introduced, except for the smallest SiO_2 NPs. Further, for each nanoparticle size, there is more lateral order and more trans bonds for DSPC compared with DPPC. The same trends are observed (not shown) from plots of $I(1121)/I(1127)$ vs $S_{lateral}$.

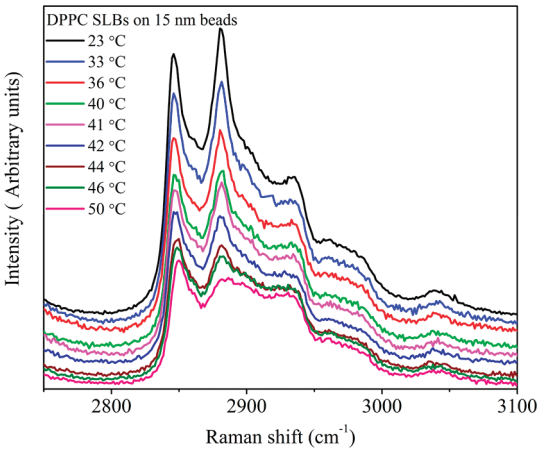

Figure 6. Temperature dependent Raman spectra of DPPC in the CH_2 and CH_3 stretching region on 15 nm SiO_2.

Correlation of rotational disorder with intermolecular interactions can also be viewed by plotting $I[(\nu_s^{FR}(CH_2,CH_3)]/I[(\nu_s^{FR}(CH_2)] = I_{2935}/I_{2845}$ versus $I[(\nu_a(CH_2)]/I[(\nu_s^{FR}(CH_2)] = I_{2884}/I_{2850}$,[23] as shown for DPPC as a function of temperature in Figure 9. Here, temperature dependent decoupling and intermolecular interactions are monitored. I_{2884}/I_{2850} is the most frequently used measure of lateral disorder, although it measures different quantities in different phases.[47] I_{2884} decreases in peak height with respect to the I_{2845}, broadens and shifts up in frequency as the chains are in a less ordered environment. I_{2935}/I_{2845} increases with increased chain decoupling (decreased intermolecular interactions) as more gauche rotamers are introduced into the chain[45] and as the terminal methyl groups have increased rotational and vibrational freedom.[47] Figure 9 shows that for all size nanoparticles, lateral disorder increases with increasing chain decoupling, induced by increases in temperature. The dashed line indicates the phase transition temperature (41.5 °C) of the DPPC MLVs.

Comparison of $S_{lateral}$ for SLBs, Alkanes, MLVs, and Interdigitated Structures. It is useful to compare order parameters for alkanes in the low temperature crystalline and high temperature melt phases, and for lipids in the low temperature gel and high temperature liquid crystalline states. Of particular interest are values for interdigitated lipids. In the low T phases, values of $S_{lateral}$ for alkanes are by definition 1.[11] In the case of DPPC, MLVs values of ~0.4 for $S_{lateral}$ at RT have been measured,[10,11,19,51,52] whereas for SUVs, $S_{lateral} \approx 0.24$.[10,11] In the current work, we have measured $S_{lateral}$ = 0.29 for the MLVs, lower than previously reported. This may be due to differences in baseline subtraction, or to freeze/thawing that decreases the MLV size. For the SLBs, $S_{lateral}$ increases from 0.24 (45 nm SiO_2)

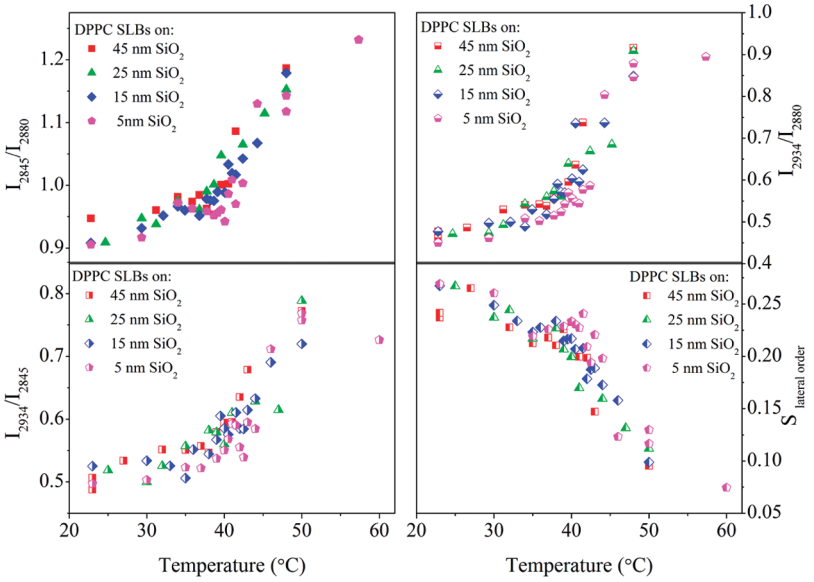

Figure 7. Plots of I_{2845}/I_{2880}, I_{2934}/I_{2884}, I_{2934}/I_{2845}, I_{2934}/I_{2880}, and $S_{lateral} = (I_{2880}/I_{2845} - 0.7)/1.5$ as a function of temperature for DPPC SLBs on 5, 15, 25, and 45 nm SiO_2.

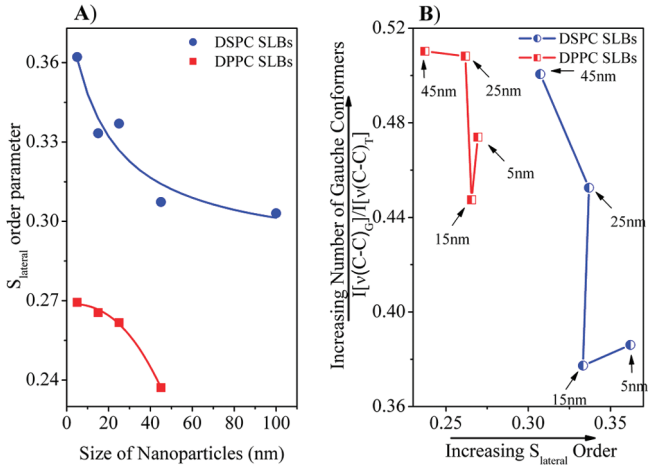

Figure 8. (A) Lateral order parameter ($S_{lateral}$) for DPPC and DSPC at RT as a function of SiO_2 size; (B) $I[\nu(C-C)_G]/I[\nu[(C-C)_T] = I_{1090}/I_{1060}$ as a function of $S_{lateral}$ for DPPC and DSPC on 40−50 (45), 20−30 (25), 10−20 (15), and 4−5 (5) nm SiO_2.

to 0.27 (5 nm SiO_2) for DPPC and from 0.30 (100 nm SiO_2) to 0.36 (5 nm SiO_2) for DSPC. These values are close to that of $S_{lateral}$ = 0.31 measured for interdigitated di-*O*-hexadecylglycerophosphocholine.[53] Greater differences in $S_{lateral}$ were observed (at T = 0 °C) between vesicles of DPPC ($S_{lateral}$ = 0.42) and fully interdigitated DPPC induced by glycerol ($S_{lateral}$ = 0.46).[19] The results in the current investigation suggest that although interdigitation increases with decreasing NP size for the SLBs, none of the structures are fully interdigitated.

In the high temperature phases, $S_{lateral}$ (alkanes) = 0, by definition. At 50 °C for DPPC, $S_{lateral}$ (0.14 for MLVs[11,51]) > $S_{lateral}$ (0.04 for SUVs[11]) > (0.03 for SLBs). This indicates that the alkanes upon melting have more conformational freedom than do SUVs or MLVs, which are constrained by their bilayer structures. Further, the melt of the SUVs and SLBs is more disordered than the melt of MLVs, indicating that more order is preserved in more planar lipid gels compared with the highly curved SUVs and SLBs, which may result from their greater free volume at melting.

The picture that emerges from the Raman data is shown schematically in Figure 3. The alkyl chains on the nanoparticle SLBs cannot adopt a bilayer structure due to the high curvature of the underlying supports. Unlike MLVs or SLVs, the inner leaflet is attached, albeit with an intervening ∼1−2 nm water layer, to the SiO_2 substrate, and it may be reasonable to assume that the headgroup of the inner layer facing the SiO_2 has a packing arrangement similar to that on planar supported bilayers. As the curvature of the underlying SiO_2 increases, the alkyl chains would have increasingly large voids between the chains, decreasing their hydrophobic interactions. This packing problem would be worse for the lipid on the outer leaflet of the bilayer. We propose that for the 100 nm SiO_2 (data could only be obtained for DSPC SLBs) this space is filled by the terminal gauche kink of the methyl groups, as indicated by the large 1122 cm^{-1} band (Figure 1). This kink fills the "void" space, but at the expense of decreased lateral packing of the chains. As the SiO_2 size decreases, and the wedge shaped "void" space increases, it becomes increasingly favorable for the two halves of the bilayer to interdigitate. Thus, as observed from the Raman data, lateral packing (as measured by $S_{lateral}$) and trans bonds (as measured by I_{1060}/I_{1090} (trans/gauche) and I_{1127}/I_{1122} (trans/gauche methyl kink)) increase with decreasing SiO_2 size. The trends for our data suggest increased interdigitation with decreasing nanoparticle size. However, although the value of $S_{lateral}$ is greater for DSPC SLBs than for DSPC MLVs (as expected for interdigitated structures), and comparable to interdigitated DHPC vesicles,[53] it is less for DPPC SLBs than for gel-phase MLV dispersions of DPPC. This can be the result of the constraints imposed by the SiO_2 substrate, and/or to only partially interdigitated structures. Increased lipid interdigitation with decreased NP size can account for the smaller than predicted diffusion coefficients of lipids on <50 nm diameter SiO_2 coated nanowires, where free space models and cylinder lipid volumes were considered.[54]

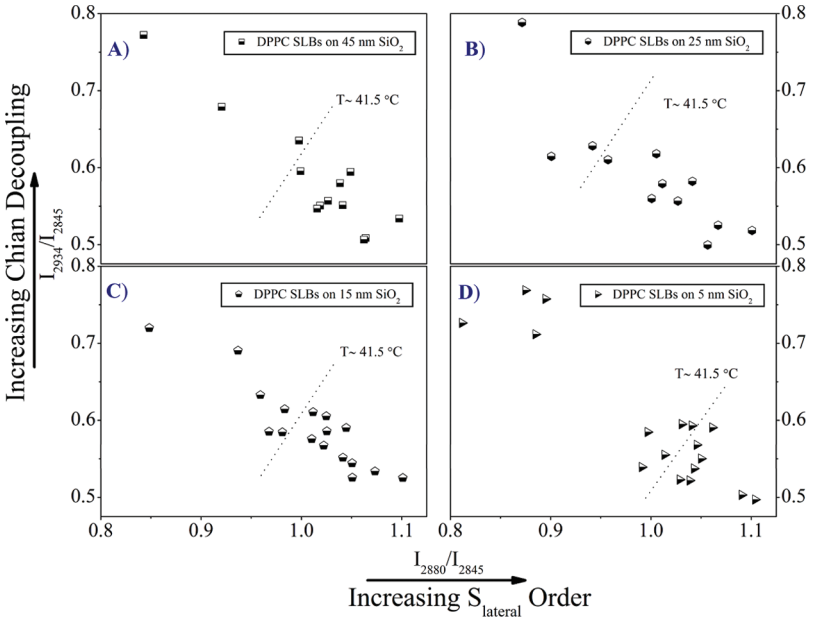

Figure 9. Plots of I_{2934}/I_{2845}, a measure of chain decoupling, versus I_{2880}/I_{2845}, a measure of lateral order, for SLBs of DPPC on 5, 15, 25, and 45 nm SiO_2, as a function of temperature. Dashed line indicates gel-to-liquid crystal phase transition temperature of DPPC MLVs.

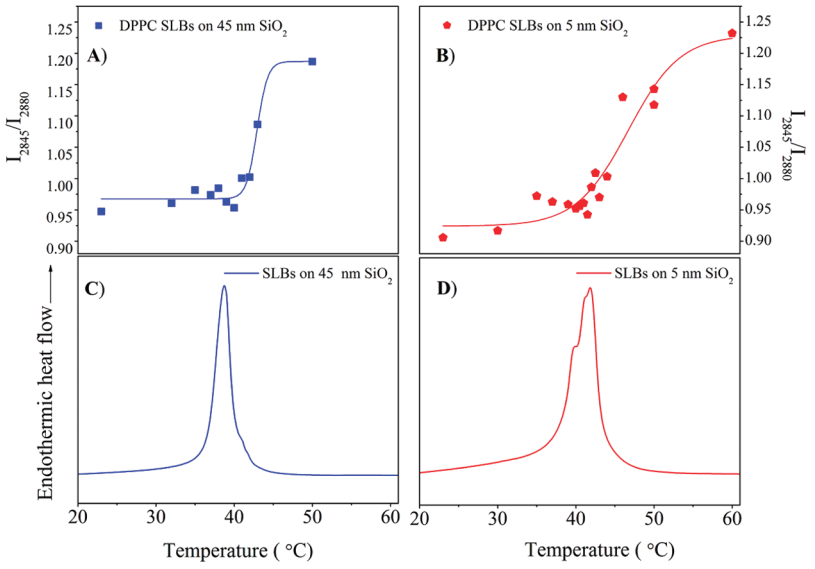

Figure 10. I_{2845}/I_{2880} versus temperature for DPPC on (A) 45 nm SiO_2 and (B) 5 nm, SiO_2. NanoDSC thermograms of the gel-to-liquid crystalline phase transition temperature for DPPC on (C) 45 nm SiO_2 and (D) 5 nm SiO_2.

The "kink" produced by the terminal methyl group persists for all size SiO_2 SLBs, but it is not possible to determine if it is on only one of the two acyl chains or preferentially on the inner or outer leaflet of the bilayer. In MD simulations of lipids in the gel phase, correlations were found between the two bilayers, such that an exceptionally ordered region of one monolayer faced an exceptionally disordered region in the opposing monolayer.[34] The observed decrease in lateral packing of SUVs compared with MLVs was suggested to arise from changes in the packing of the chains toward the center of the bilayers.[12] In view of the assignment of the 1121 cm^{-1} vibration to the gauche bond rotation of the terminal methyl group (i.e., at the bilayer center), this conformation cannot then also contribute to the broad gauche 1090 cm^{-1} mode. The conformations contributing to this band are thus more likely due to gauche conformers (Figure 3) that maintain the orientation of the acyl chains in a direction normal to surface of the bilayer.[55,56]

Smallest (4−5 nm) SLBs. As discussed above, the trends observed for I_{1090}/I_{1060} (gauche/trans) and I_{1121}/I_{1127} (terminal gauche/trans) (Figure 2) do not apply for the smallest (5 nm SiO_2) nanoparticles, although the smallest NP does follow the trend for lateral packing order (Figure 8). Unlike the 15, 25, 45, and 100 nm SLBs, where a single SLB was observed to surround each nanoparticle,[18,57,58] consistent with other reported data,[59] dynamic light scattering (DLS) showed that the 5 nm SLBs formed large aggregates.[57] This suggests that the lipids on the

5 nm SiO_2 form both interdigitated SLBs and extended networks of bridged NPs, in which each half of the bilayer is on an adjacent NP, accounting for the high lateral packing order (Figure 10). Loosely packed or isolated chains in the interstitial regions could account for the slight increase in gauche bonds and chains with gauche defects at the terminal methyl groups for the 5 compared with 15 nm SLBs. This structure is also suggested by the different behavior (Figure 9) observed for the 5 nm SiO_2 when chain decoupling, reflecting both gauche rotamers and dynamics, is plotted versus lateral order parameter. There is a more abrupt change in this ratio, and it occurs at a higher temperature, for the 5 nm SLBs than for the other SiO_2 sizes. Similarly, the gel-to-liquid crystalline transition, monitored by Raman spectroscopy, occurs at a higher temperature and over a broader temperature range, for the 5 compared with the 15, 25, and 45 nm SLBs, as reported previously[18] and shown along with nanodifferential scanning calorimetry data that exhibit the same behavior (Figure 10).

These results suggest that the lipids on the 5 nm SLB aggregates remain in contact to higher temperatures than for SLBs in which the chains undergo the gel-to-liquid transition on individual SiO_2 NPs. Chains in contact as the result of lipid bridges, as shown schematically in Figure 3F, may require higher temperatures to melt. Extended networks of interdigitated structures have also been proposed for alkane thiols on 1.2 nm gold (Au) particles[60] and fatty acids on silver (Ag) colloids,[61] and mixtures of ordered intercalated chains along with mobile, isolated chains located at interstitial regions between the particles have been suggested for Au colloids.[62]

Lastly, we note that the 5 and 15 nm SLBs are more similar to each other (e.g., Figures 2A and 8B), than they are to the larger SLBs. Although for suspended SLBs, obtained at low ionic strengths, we only observed aggregates/clusters for the 5 nm SLBs,[57] it is possible that aggregates/clusters form for the 15 nm SLBs at the high ionic strengths used in this investigation. However, at these ionic strengths, precipitation occurs for all size SLBs, precluding DLS analysis. Experimentally, there is a critical NP size (~20 nm) below which it appears difficult to form a single SLB around a NP[59] and theoretical models indicate that as the NP size reaches a critical value, there is unbinding (no wrapping) or partial wrapping[63] of the vesicle around the NP, since the energy gain due to adhesion can no longer compensate for the cost of bending and stretching the membrane.[64] Both the 5 and 15 nm SLBs may have some amount of aggregation, involving lipid bridging. It is also possible that supported lipid bilayers could form around NP clusters, but previous thermogravimetric analysis data showed good agreement between the mass of lipid measured and that expected based on a single SLB around each SiO_2 NP, except for the 5 nm SLBs.[18] In the latter case, it is also possible that the lipid forms a SLB over a group of SiO_2 NPs, but further experiments are need to indicate the morphology of these aggregates/clusters. For the larger NPs, where full wrapping is expected,[64] terminal gauche defects become more prominent as a means of filling the void space.

It is very likely that the environment for lipids on high curvature supports is heterogeneous. The Raman results have been interpreted in a manner that by necessity is too simplified. The Raman spectra reflect average values of the conformational and packing properties of the lipids and cannot discern local heterogeneities in the lipid structure.

CONCLUSIONS

Conformational order and alkyl chain packing of supported lipid bilayers (SLBs) of phosphatidyl choline (PC) lipids with different alkyl chain lengths (C_{16} and C_{18}) on SiO_2 nanoparticles with sizes between 5 and 100 nm were studied by Raman spectroscopy. There are major differences found in the intrachain (trans−gauche) and interchain (lateral packing) of the alkyl chains of the SLBs as a function of NP size. This is shown by ν(C−C) and ν(C−H) stretching modes of the adsorbed lipids on the surface of the nanoparticles. The hydrocarbon chains of SLBs have more highly ordered, trans chain conformations (lower values of I_{1090}/I_{1060} and I_{1121}/I_{1127}) on smaller size (15 nm) nanoparticles, with the chains becoming more disordered in terms of lateral packing and gauche defects with increasing bead size (100 nm). Further, for the same size NP, the chains are more disordered for the shorter (DPPC, 16 carbon) compared with the longer alkyl (DSPC, 18 carbon) chain lipid. These results were interpreted as arising from increased interdigitation of the alkyl chains as their dimensions approached those of the NPs, and arose from the necessity of avoiding the high free volume that would result from a bilayer structure, which would expose the hydrophobic chains to an aqueous environment. Another way to fill this free volume, and increase hydrophobic interactions, was the formation of chains with a single gauche defect (1122 cm^{-1} vibration) at the terminal methyl group. The smallest, 5 nm SLBs, formed aggregates, in which we propose that bilayer bridging can occur.

ABBREVIATIONS

SiO_2: silica
NP: nanoparticle
DSPC: 1,2-distearoyl-*sn*-glycero-3-phosphocholine
DPPC: 1,2-dipalmitoyl-*sn*-glycero-3-phosphocholine
DMPC: 1,2- dimyristoyl- *sn*-glycero-3-phosphocholine
SLB: supported lipid bilayer
MLV: multilamellar vesicle
SUV: small unilamellar vesicle
nano-DSC: nanodifferential scanning calorimetry
RT: room temperature
FR: Fermi resonance
DLS: dynamic light scattering

REFERENCES

(1) Larsson, K. *Chem. Phys. Lipids* **1973**, *10*, 165–176.
(2) Larsson, K.; Rand, R. P. *Biochim. Biophys. Acta, Lipids Lipid Metab.* **1973**, *326*, 245–55.
(3) Spiker, R. C., Jr.; Levin, I. W. *Biochim. Biophys. Acta, Lipids Lipid Metab.olism* **1975**, *388*, 361–73.
(4) Lippert, J. J. L.; Peticola, Wl *Biochim. Biophys. Acta* **1972**, *282*, 8–&.
(5) Lippert, J. L.; Peticola, W. L. *Proc. Natl. Acad. Sci. U.S.A.* **1971**, *68*, 1572.
(6) Yellin, N.; Levin, I. W. *Biochim. Biophys. Acta* **1977**, *489*, 177–190.
(7) Lee, C. S.; Bain, C. D. *Biochim. Biophys. Acta-Biomembr.* **2005**, *1711*, 59–71.
(8) Sweetenham, C. S.; Notingher, I. *Spectrosc. Int. J.*, *24*, 113-117.
(9) Spiker, R. C.; Levin, I. W. *Biochim. Biophys. Acta* **1976**, *433*, 457–468.
(10) Spiker, R. C.; Levin, I. W. *Biochim. Biophys. Acta* **1976**, *455*, 560–575.

(11) Gaber, B. P.; Peticolas, W. L. *Biochim. Biophys. Acta, Biomembr.* **1977**, *465*, 260–74.
(12) Mendelsohn, R.; Sunder, S.; Bernstein, H. J. *Biochim. Biophys. Acta, Biomembr.* **1976**, *419*, 563–9.
(13) Gaber, B. P.; Sheridan, J. P. *Biochim. Biophys. Acta* **1982**, *685*, 87–93.
(14) Chang, E. L.; Gaber, B. P.; Sheridan, J. P. *Biophys. J.* **1982**, *39*, 197–201.
(15) Suurkuusk, J.; Lentz, B. R.; Barenholz, Y.; Biltonen, R. L.; Thompson, T. E. *Biochemistry* **1976**, *15*, 1393–1401.
(16) Boni, L. T.; Minchey, S. R.; Perkins, W. R.; Ahl, P. L.; Slater, J. L.; Tate, M. W.; Gruner, S. M.; Janoff, A. S. *Biochim. Biophys. Acta* 1993, *1146*, 247-57.
(17) Slater, J. L.; Huang, C. H. *Prog. Lipid Res.* **1988**, *27*, 325–59.
(18) Ahmed, S.; Wunder, S. L. *Langmuir* **2009**, *25*, 3682–3691.
(19) Oleary, T. J.; Levin, I. W. *Biochim. Biophys. Acta* **1984**, *776*, 185–189.
(20) Slater, J. L.; Huang, C. H.; Levin, I. W. *Biochim. Biophys. Acta* **1992**, *1106*, 242–250.
(21) Yellin, N.; Levin, I. W. *Biochemistry* **1977**, *16*, 642–647.
(22) Akutsu, H. *Biochemistry* **1981**, *20*, 7359–7366.
(23) Orendorff, C. J.; Ducey, M. W.; Pemberton, J. E. *J. Phys. Chem. A* **2002**, *106*, 6991–6998.
(24) Meier, R. J.; Csiszar, A.; Klumpp, E. *J. Phys. Chem. B* **2006**, *110*, 5842–5844.
(25) Tasumi, M.; Shimanouchi, T. *J. Mol. Spectrosc.* **1962**, *9*, 261–&.
(26) Schachtschneider, J. H.; Snyder, R. G. *Spectrochim. Acta* **1963**, *19*, 117–168.
(27) Snyder, R. G.; Schachtschneider, J. H. *Spectrochim. Acta* **1963**, *19*, 85–116.
(28) Levin, I. W. In *Advances in Infrared and Raman Spectroscopy*; Clark, R. J. H., Hester, R. E., Eds.; Wiley Heyden: New York, 1984; Vol. 11, pp 1−48.
(29) Maroncelli, M.; Strauss, H. L.; Snyder, R. G. *J. Chem. Phys.* **1985**, *82*, 2811–2824.
(30) Snyder, R. G. *J. Chem. Phys.* **1967**, *47*, 1316–&.
(31) Meier, R. J. *Polymer* **2002**, *43*, 517–522.
(32) Koglin, E.; Meier, R. J. *Comput. Theor. Polym. Sci.* **1999**, *9*, 327–333.
(33) Snyder, R. G.; Cameron, D. G.; Casal, H. L.; Compton, D. A. C.; Mantsch, H. H. *Biochim. Biophys. Acta* **1982**, *684*, 111–116.
(34) Snyder, R. G.; Tu, K. C.; Klein, M. L.; Mendelssohn, R.; Strauss, H. L.; Sun, W. J. *J. Phys. Chem. B* **2002**, *106*, 6273–6288.
(35) Savarala, S.; Monson, F.; Ilies, M. A.; Wunder, S. L. *Langmuir* **2011**, *27*, 5850–5861.
(36) Lavialle, F.; Levin, I. W.; Mollay, C. *Biochim. Biophys. Acta* **1980**, *600*, 62–71.
(37) Stockton, G. W.; Polnaszek, C. F.; Tulloch, A. P.; Hasan, F.; Smith, I. C. P. *Biochemistry* **1976**, *15*, 954–966.
(38) Zerbi, G.; Magni, R.; Gussoni, M.; Moritz, K. H.; Bigotto, A.; Dirlikov, S. *J. Chem. Phys.* **1981**, *75*, 3175–3194.
(39) Snyder, R. G.; Hsu, S. L.; Krimm, S. *Spectrochim. Acta Part a-Mol. Biomol. Spectrosc.* **1978**, *34*, 395–406.
(40) Abbate, S.; Zerbi, G.; Wunder, S. L. *J. Phys. Chem.* **1982**, *86*, 3140–3149.
(41) Boerio, F. J.; Koenig, J. L. *J. Chem. Phys.* **1970**, *52*, 3425–&.
(42) Hill, I. R.; Levin, I. W. *J. Chem. Phys.* **1979**, *70*, 842–851.
(43) Macphail, R. A.; Strauss, H. L.; Snyder, R. G.; Elliger, C. A. *J. Phys. Chem.* **1984**, *88*, 334–341.
(44) Cho, Y.; Kobayashi, M.; Tadokoro, H. *J. Chem. Phys.* **1986**, *84*, 4636–4642.
(45) Wunder, S. L.; Bell, M. I.; Zerbi, G. *J. Chem. Phys.* **1986**, *85*, 3827–3839.
(46) Snyder, R. G.; Scherer, J. R. *J. Chem. Phys.* **1979**, *71*, 3221–3228.
(47) Snyder, R. G.; Strauss, H. L.; Elliger, C. A. *J. Phys. Chem.* **1982**, *86*, 5145–5150.
(48) Snyder, R. G.; Scherer, J. R.; Gaber, B. P. *Biochim. Biophys. Acta* **1980**, *601*, 47–53.
(49) Huang, C. H.; Lapides, J. R.; Levin, I. W. *J. Am. Chem. Soc.* **1982**, *104*, 5926–5930.
(50) Fox, C. B.; Uibel, R. H.; Harris, J. M. *J. Phys. Chem. B* **2007**, *111*, 11428–11436.
(51) Bunow, M. R.; Levin, I. W. *Biochim. Biophys. Acta* **1977**, *487*, 388–394.
(52) Karvaly, B.; Loshchilova, E. *Biochim. Biophys. Acta, Biomembr.* **1977**, *470*, 492–6.
(53) Lewis, E. N.; Bittman, R.; Levin, I. W. *Biochim. Biophys. Acta* **1986**, *861*, 44–52.
(54) Huang, S. C. J.; Artyukhin, A. B.; Martinez, J. A.; Sirbuly, D. J.; Wang, Y.; Ju, J. W.; Stroeve, P.; Noy, A. *Nano Lett.* **2007**, *7*, 3355–3359.
(55) Liu, J.; Conboy, J. C. *J. Phys. Chem. C* **2007**, *111*, 8988–8999.
(56) Seelig, A.; Seelig, J. *Biochemistry* **1974**, *13*, 4839–4845.
(57) Savarala, S.; Ahmed, S.; Ilies, M. A.; Wunder, S. L. *Langmuir* **2010**, *26*, 12081–12088.
(58) Savarala, S.; Ahmed, S.; Ilies, M. A.; Wunder, S. L. *ACS Nano* **2011**, *5*, 2619–2628.
(59) Roiter, Y.; Ornatska, M.; Rammohan, A. R.; Balakrishnan, J.; Heine, D. R.; Minko, S. *Langmuir* **2009**, *25*, 6287–6299.
(60) Terrill, R. H.; Postlethwaite, T. A.; Chen, C. H.; Poon, C. D.; Terzis, A.; Chen, A. D.; Hutchison, J. E.; Clark, M. R.; Wignall, G.; Londono, J. D.; Superfine, R.; Falvo, M.; Johnson, C. S.; Samulski, E. T.; Murray, R. W. *J. Am. Chem. Soc.* **1995**, *117*, 12537–12548.
(61) Patil, V.; Mayya, K. S.; Pradhan, S. D.; Sastry, M. *J. Am. Chem. Soc.* **1997**, *119*, 9281–9282.
(62) Badia, A.; Gao, W.; Singh, S.; Demers, L.; Cuccia, L.; Reven, L. *Langmuir* **1996**, *12*, 1262–1269.
(63) Fleck, C. C.; Netz, R. R. *Europhys. Lett.* **2004**, *67*, 314–320.
(64) Deserno, M.; Gelbart, W. M. *J. Phys. Chem. B* **2002**, *106*, 5543–5552.